Research Square

Preprints are preliminary reports that have not undergone peer review.
They should not be considered conclusive, used to inform clinical practice,
or referenced by the media as validated information.

Virtual screening and mechanism research of anti-tumor active ingredients from Sarcandra glabra targeting VEGFR-2

Wen Xing

1197724985@qq.com

Shenyang Institute of Science and Technology

Guo-Zhu Gao

Shenyang Institute of Science and Technology

Fang-Yuan Ji

Shenyang Institute of Science and Technology

Zhen-Yu Kuai

Maanshan technical college

Yan-Qiu Meng

Research Article

Keywords: Sarcandra glabra, VEGFR 2, molecular docking, virtual screening, surface plasmon resonance, druggability

Posted Date: October 19th, 2026

DOI: https://doi.org/10.21203/rs.3.rs-11117664/v1

License: This work is licensed under a Creative Commons Attribution 4.0 International License.
Read Full License

Additional Declarations: No competing interests reported.

Virtual screening and mechanism research of anti-tumor active ingredients from *Sarcandra glabra* targeting VEGFR-2

Wen Xing[a], Guo-Zhu Gao[a], Fang-Yuan Ji[a],Zhen-Yu Kuai[b] and Yan-Qiu Meng[c]

[a]Shenyang Institute of Science and Technology, Shenyang 110167,China;[b]Department of Pharmacy teaching and research, Maanshan technical college, Maanshan 243031,china; [C]Shenyang University of Chemical Technology, Shenyang 110142,China

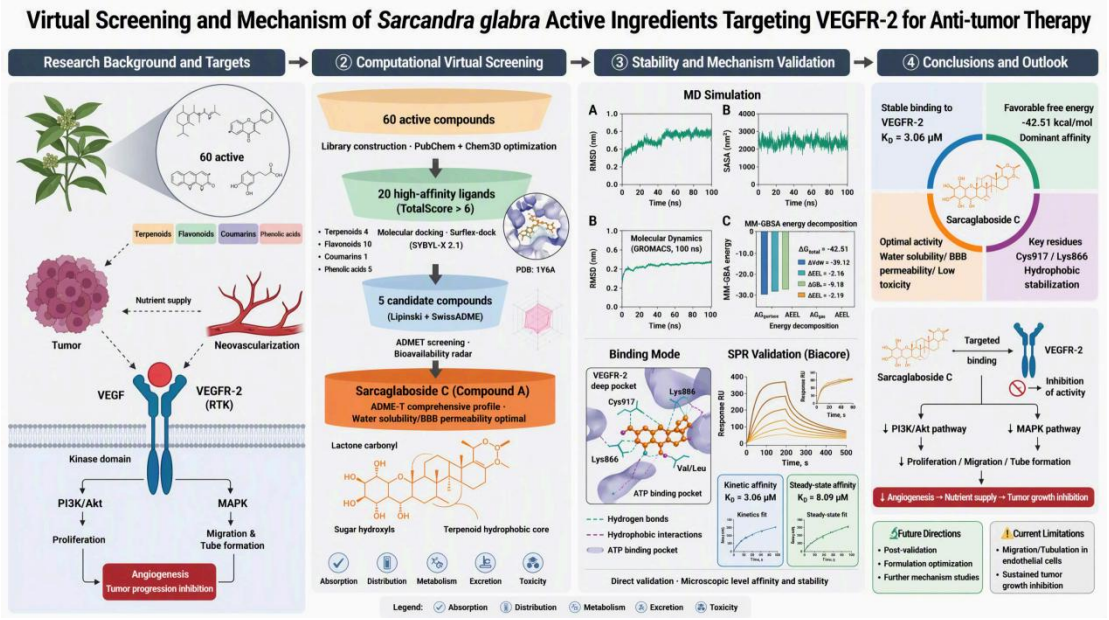
ABSTRACT

In this study, computer-aided drug design techniques were employed to screen antitumor active ingredients from Sarcandra glabra that target vascular endothelial growth factor receptor-2 (VEGFR-2), and to elucidate the binding mode and druggability potential of promising candidate compounds for this target protein. Molecular docking was performed with the Surflex-dock module in SYBYL-X2.1 software, and ligands exhibiting high binding affinity were screened using a TotalScore threshold of greater than 6. Lipinski's Rule of Five combined with the SwissADME platform was applied for preliminary druglikeness screening. SwissADME and Discovery Studio 2019 Client were further utilized to predict ADME-T pharmacokinetic and toxic properties. Molecular dynamics simulations of Sarcaglaboside C, the optimal compound obtained through comprehensive screening, were performed via GROMACS software to evaluate its binding stability with VEGFR-2. Meanwhile, surface plasmon resonance (SPR) assays were carried out to verify the binding capacity between the compound and VEGFR-2 at the in-vitro molecular level. The results showed that Sarcaglaboside C exhibited strong binding affinity toward VEGFR-2 protein, with a kinetic-fitted KD of 3.06 μM and a steady-state-fitted KD of 8.09 μM. Additional molecular-docking analysis characterized its interaction pattern, revealing that multiple hydroxyl groups of this compound could form hydrogen-bond interactions with amino-acid residues of VEGFR-2. Taken together, Sarcaglaboside C, a terpenoid compound derived from Sarcandra glabra, can stably bind to VEGFR-2 protein. These findings suggest that this compound possesses antitumor potential by targeting VEGFR-2 and may serve as a lead compound for follow-up structural-optimization investigations.

Keywords: Sarcandra glabra; VEGFR-2; molecular docking; virtual screening; surface plasmon resonance; druggability

CONTACT Wen Xing,1197724985@qq.com,Shenyang Institute of Science and Technology, Shenyang 110167, China

Graphical Abstract



1.Introduction

Sarcandra glabra, the dried whole herb of *Sarcandra glabra* (Chloranthaceae family), is a commonly-used traditional Chinese medicine with anti-tumor effects in clinical practicePMC. It is documented in traditional Chinese medicine records for dissipating masses and eliminating concretions. Modern pharmacological studies have verified that *Sarcandra glabra* possesses multiple pharmacological activities including inhibiting tumor proliferation, inducing tumor-cell apoptosis, suppressing invasion and metastasis, regulating body immunity, and alleviating toxic and side-effects of radiotherapy and chemotherapy. It is widely applied in adjuvant therapy for solid tumors such as lung cancer, gastric cancer and liver cancer [1].*Sarcandra glabra* is rich in terpenoids, flavonoids, coumarins, phenolic acids, polysaccharides and other active substances. Existing researches mostly focus on the overall pharmacological evaluation of crude extracts. Nevertheless, the core active monomer components, direct action targets and molecular interaction mechanisms responsible for its anti-tumor effects remain unclear, which restricts the development and clinical transformation of targeted innovative drugs derived from *Sarcandra glabra*.

Pathological tumor angiogenesis acts as a core link for tumor proliferation, invasion and distant metastasis, providing essential nutritional supply and anatomical channels for tumor growth, progression and metastatic colonization. Vascular endothelial growth factor receptor-2 (VEGFR-2), a key member of the receptor tyrosine kinase (RTK) family, serves as the central target for angiogenesis regulation [2]. After vascular endothelial growth factor (VEGF) specifically binds to VEGFR-2 on cell-membrane surface, classic pro-angiogenic signaling pathways such as PI3K/Akt and MAPK become activated, mediating abnormal proliferation, migration and tube-formation of vascular endothelial cells and triggering massive generation of tumor neovessels. Therefore, specifically blocking VEGFR-2 kinase activity and inhibiting pathological tumor angiogenesis can arrest tumor progression through the “nutrient deprivation” strategy, which represents an important research direction for current anti-tumor targeted therapy

[3]. Although clinically-used VEGFR tyrosine-kinase-targeted drugs such as imatinib and sunitinib exhibit definite therapeutic efficacy, they are accompanied by severe toxic side-effects and high risks of drug resistance. Compared with chemically-synthesized targeted drugs, natural small-molecule compounds originating from traditional Chinese medicine possess unique advantages of low toxicity, structural diversity and multi-target synergistic effects. They constitute a high-quality natural screening library for novel potent and low-toxic VEGFR-2-targeted inhibitors.

Computer-aided drug design covers technologies including molecular docking, virtual screening and ADMET prediction. It enables efficient assessment of target-binding affinity, drug-likeness filtering and druggability risk prediction for natural products, greatly shortening drug-research-and-development cycles and lowering research costs. It has become a core technical tool for excavating lead compounds from traditional-Chinese-medicine sources and elucidating molecule-target interaction mechanisms [4]. On this basis, the present study took VEGFR-2 as the anti-tumor target. A natural ligand compound library was constructed by collecting 60 reported monomer active ingredients from *Sarcandra glabra*. Multi-dimensional evaluations including molecular-docking-based virtual screening, Lipinski's drug-likeness rule assessment and ADME-T druggability prediction were performed to screen out superior compounds. The interaction modes between candidate small molecules and VEGFR-2 target protein were analyzed, and the potential molecular pharmacological mechanism whereby *Sarcandra glabra* targets VEGFR-2 to suppress tumor angiogenesis was interpreted. This study provides theoretical support for exploring potent, low-toxic anti-tumor lead compounds and developing innovative drugs originating from *Sarcandra glabra*.

2. Instruments and Materials

Relevant Chinese and English literature on chemical constituents of *Sarcandra glabra* were retrieved, and a total of 60 reported active monomers belonging to four categories (terpenoids, flavonoids, coumarins and phenolic acids) were collected. Small-molecule structures were downloaded from the PubChem database and imported into Chem3D software for energy minimization optimization to construct a dedicated ligand small-molecule library for *Sarcandra glabra*. The crystal model of the VEGFR-2 kinase domain (PDB ID: 1Y6A) [5] was downloaded from the RCSB-PDB database. The SwissADME web server was used for drug-likeness and ADME prediction. SYBYL-X 2.1 software and Discovery Studio 2019 Client software were adopted for molecular docking and virtual screening (Table 1).

Table 1 Basic information of small-molecule ligand library of active ingredients

No.	Name	Classification	PubChem CID
1	Atractylenolide II	Terpenoids	14448070
2	Atractylenolide III	Terpenoids	155948
3	Chloranthalactone A	Terpenoids	333361
4	Chloranthalactone B	Terpenoids	15767607
5	Chloranthalactone E	Terpenoids	131676069
6	Chloranthalactone F	Terpenoids	274030919
7	Chloranthalactone G	Terpenoids	102247108
8	Chloranthalactone E 8-O-β-D-glucopyranosid	Terpenoids	11647529

9	Chloranoside A	Terpenoids	11962123
10	Furanodienone	Terpenoids	179413
11	（-）-Istanbulin A	Terpenoids	12304519
12	（-）-Istanbulin B	Terpenoids	131751897
13	Lupeol	Terpenoids	259846
14	Nerolidol	Terpenoids	5284507
15	Sarcaglaboside A	Terpenoids	11546034
16	Sarcaglaboside B	Terpenoids	11545986
17	Sarcaglaboside C	Terpenoids	11596696
18	Sarcaglaboside E	Terpenoids	11526742
19	Sarcaglaboside F	Terpenoids	42604346
20	Shizukanolide A	Terpenoids	333362
21	Spathulenol	Terpenoids	10207
22	GlabraosideA	Flavonoids	102393599
23	GlabraosideB	Flavonoids	275663462
24	Catechin 3-O-α-L-rhamnopyranoside	Flavonoids	44257078
25	2',4' -dihydroxy-6'-methoxydihydrochalcone	Flavonoids	6483649
26	2',4'-dihydroxy-4,6'-dimethoxydihyrochalcone	Flavonoids	637162
27	2',6'-dihydroxy-4'-methoxydihydrochalcone	Flavonoids	169676
28	2',6'-dihydroxy-4,4'-dimethoxydihydrochalcone	Flavonoids	3084606
29	2'-hydroxy-4',6'-dimethoxydihydrochalcone	Flavonoids	67218245
30	2'-hydroxy-4.4',6'-trimethoxydihydrochalcone	Flavonoids	270057
31	2',4',4-Trihydroxychalcone	Flavonoids	5281278
32	5-Hydroxy-7,4'-dimethoxydihydroflavanone	Flavonoids	14057196
33	4',5-dibydroxy-7-methoxyflavanone	Flavonoids	143657
34	（+）-3,3',5,5',7-pentahydroxyflavanone	Flavonoids	97032110
35	3,3',4',5,7-pentahydroxyflavone	Flavonoids	5280343
36	Kaempferol-3-0-β-D-glucuronide	Flavonoids	5280648
37	Quercetin-3-0-α-D-glucuronide	Flavonoids	5274585
38	Quercetin-3-O-β-D-glucuronopyranoside methyl ester	Flavonoids	21722016
39	Neoastilbin	Flavonoids	101741
40	5,7,3',4'-tetrahydroxy-6-C-β-D-glucopyranosylflavanone	Flavonoids	3082645
41	4,4'-Biisofraxidin	Coumarins	11259276
42	Esculetin	Coumarins	5281416
43	Fraxetin	Coumarins	5281459
44	Scoparone	Coumarins	14680
45	Isofraxidin	Coumarins	5281628
46	Scopoletin	Coumarins	5281460
47	Eleutheroside B_1	Coumarins	143645
48	Fraxidin5316860	Coumarins	101751
49	Coumarin	Coumarins	323
50	Isofraxidin-7-O-β-D-glucopyranoside	Coumarins	5318566
51	Caffeic acid	Phenolic acids	689043
52	Rosmarinic acid	Phenolic acids	5281792
53	Methyl rosmarinate	Phenolic acids	6479915
54	3,4-Dihydroxybenzoic acid	Phenolic acids	72
55	Dibutyl phthalate	Phenolic acids	3026
56	Ethyl rosmarinate	Phenolic acids	44437692
57	4'-O-β-D-glycopyranosyl rosmarinic acid	Phenolic acids	10414396
58	Evofolin-A	Phenolic acids	12181418
59	Methyl α,3,4-trihydroxy benzenepropanoate	Phenolic acids	10584634
60	Ferulic acid	Phenolic acids	445858

Main instruments: Biacore instrument (Model: 1K, Cytiva); Pipettes (1 mL/200 μL/100 μL/10 μL/ 2 μL, Cytiva); Vortex mixer (VORTEX 06, IKA); Mini centrifuge (PPDniSpinL, Eppendorf); CM5 sensor chip (BR-1005-30, Cytiva); 10 × PBS-P+ running buffer (28995084, Cytiva);

Amine-coupling kit (BR100050, Cytiva); DMSO (D8418, Sigma-Aldrich); Sdium-acetate buffers (pH 4.0/4.5/5.0, BR100349, Cytiva).

3. Methods

3.1 Preparation and optimization of receptor-protein model

The VEGFR-2 kinase-domain crystal with PDB ID 1Y6A (crystal diffraction resolution 1.90 Å) was selected as target protein for molecular docking. Protein preparation was completed under the Docking suite module in SYBYL-X2.1 software, including protein repair, water-molecule removal, hydrogen-atom supplementation, assignment of heteroatom charges and bond orders. Energy minimization optimization for the whole protein structure was performed via the Minimization module to obtain a structural model closer to native physiological conformation [6].

3.2 Molecular-docking-based virtual screening

The Surflex-dock module within SYBYL-X2.1 software was used for molecular docking. The ATP-binding active pocket of the VEGFR-2 kinase domain was selected as the acting region to construct the Protomol with unified docking parameters. The TotalScore function built in software was applied to evaluate ligand-receptor binding affinity. The screening threshold was set as TotalScore＞6 [7], high-affinity candidate small molecules were retained, and docking-score distributions of various compounds were statistically analyzed.

3.3 Drug-likeness screening

High-affinity ligands obtained from docking screening were imported to the SwissADME platform to calculate physicochemical parameters: molecular weight (MW), hydrogen-bond donors (HBD), hydrogen-bond acceptors (HBA), lipophilic partition coefficient (LogP), topological polar-surface area (TPSA). Lipinski's Rule of Five for oral drugs was followed. Candidates with oral druggability potential were screened according to lipophilicity, molecular size, polarity, solubility, flexibility and saturation.

3.4 ADME-T pharmacokinetic and toxicity prediction

SwissADME together with the Small Molecules module of Discovery Studio 2019 Client were combined to perform ADME-T parameter prediction for candidate compounds. For absorption, compound solubility was calculated using three different approaches: the Estimated Solubility (ESOL) equation for organic-salt solubility prediction, aqueous-log-solubility index (ALI), and SILICOS-IT in-silico structural index. P-glycoprotein (P-gp) substrate properties were predicted simultaneously. For distribution, blood-brain-barrier penetration grade LogBBB and blood-brain-barrier penetration surface-area logarithm LogPS were assessed. For metabolism, inhibition effects against five major subtypes of key drug-metabolizing cytochrome P450 enzymes (CYP1A2, CYP2C9, CYP2C19, CYP2D6, CYP3A4) were mainly evaluated. For excretion and toxicity, organic-cation-transporter-2 (OCT2) substrate characteristics and potential hepatotoxicity

risks were predicted. Druggability profiles of candidate compounds were summarized based on above parameters.

3.5 Molecular-dynamics simulation

GROMACS software was used for MD simulation. The CHARMM36 all-atom force-field described protein parameters, while Sobtop combined with the GAFF force-field generated ligand topology and force-field parameters. The VEGFR-2/Sarcaglaboside-C complex model obtained from molecular docking was solvated in a cubic periodic water box, ensuring that the minimal distance between complex atoms and box walls exceeded 10 Å. The system contained adequate water molecules, and Na^+ and Cl^- ions were supplemented to neutralize net charge. MD-simulation parameter settings were as follows: two-step energy-minimization optimization was performed for conformational relaxation. Afterwards, the system was gradually heated up to 300 K, followed by sequential NVT and NPT ensemble equilibrium simulations; positional restraints were applied to stabilize conformations during equilibrium. Restraints were removed for productive MD sampling, with total simulation duration of 100 ns and time-step of 2 fs. The LINCS algorithm constrained hydrogen bonds; particle-mesh-Ewald (PME) method handled long-range electrostatic interactions. The van-der-Waals cutoff radius was set as 10 Å. Simulation trajectories were saved every 5000 simulation steps.

3.6 Affinity and activity analysis via surface-plasmon-resonance assay

A Biacore system equipped with CM5 sensor chip was applied for SPR experiments. Protein-coupling-condition screening was implemented first. VEGFR-2 stock solution was diluted with sodium-acetate buffers of different pH values. The Biacore pre-enrichment system detected response signals of VEGFR-2 under varied pH, and pH 4.5 was determined as the optimal coupling pH. Chip-surface immobilization was then conducted: mixed solution of 0.4 M EDC and 0.1 M NHS was injected over flow channels at flow-rate of 10 μL/min for 420 s to activate carboxymethyl-dextran groups on chip surfaces. VEGFR-2 protein was diluted to 50 μg/mL with 10 mM sodium-acetate buffer (pH 4.5), and injected for 420 s at identical flow-rate. VEGFR-2 protein was covalently coupled onto chip surfaces through carboxyl-amino condensation reaction. Residual activated groups were subsequently blocked by injecting 1 M ethanolamine-hydrochloride (pH 8.5) for 420 s. Test small-molecule compounds were dissolved in dimethyl sulfoxide (DMSO), then serially diluted using running buffer containing 1 % DMSO to prepare sample series with concentrations ranging from 25 nM to 25 600 nM, which were transferred to 96-well plates for on-chip detection. Binding time was set as 100 s and dissociation time as 120 s. After each detection cycle, chips were regenerated with 10 mM glycine-hydrochloride (pH 2.0) for 5 min before next-round measurement. Response values generated upon sample flowing over immobilized VEGFR-2 protein surfaces were collected. Kinetic curves were fitted according to quantitative correlation between compound concentrations and binding-response signals, so as to evaluate binding-affinity strength between small-molecule candidates and VEGFR-2 protein.

3.7 Docking analysis and image processing

The Receptor-Ligand Interactions module within Discovery Studio software was used to analyze interaction patterns between high-affinity molecules and target protein residues.

4. Results

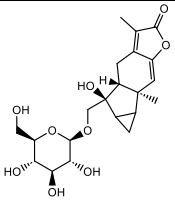
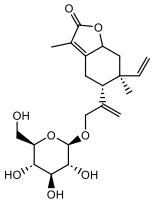
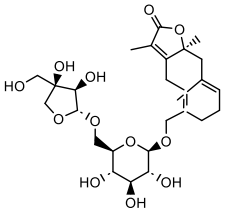
4.1 Pre-processing of VEGFR-2 protein model

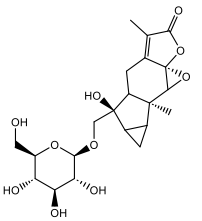
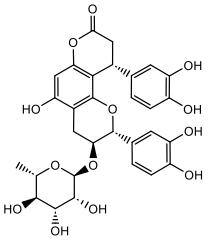
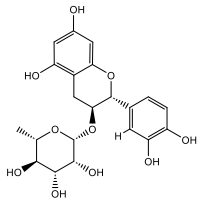
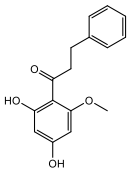
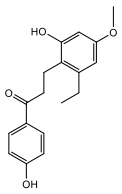
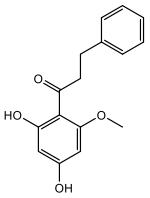
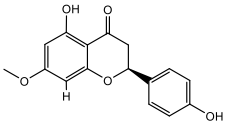
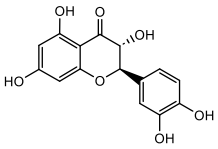
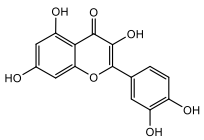
The VEGFR-2-kinase-domain crystal deposited in the RCSB-PDB database (PDB ID 1Y6A, X-ray diffraction resolution 2.10 Å) was adopted, with high crystal quality and intact active-pocket conformation. The raw crystal structure was imported to SYBYL-X2.1 software for protein repair, crystalline-water removal, hydrogen-atom addition, charge and bond-order assignment. Energy-minimization optimization was further performed to eliminate unreasonable atomic steric contacts, yielding the receptor model for subsequent virtual screening, molecular docking and molecular-dynamics simulation. Given the high diffraction resolution of raw crystal and post-optimized energy-minimization results, the VEGFR-2 receptor model possessed reasonable conformation and was applicable for follow-up computational studies.

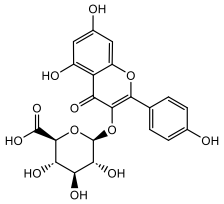
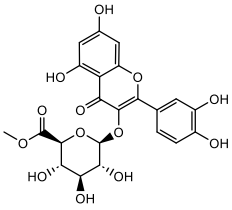
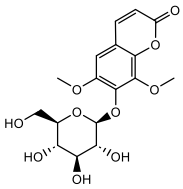
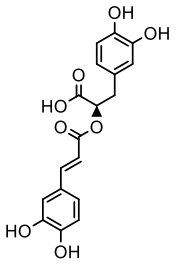
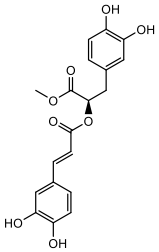
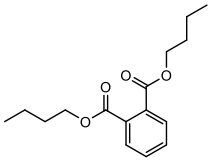
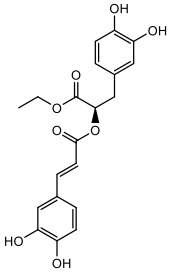
4.2 Molecular-docking results

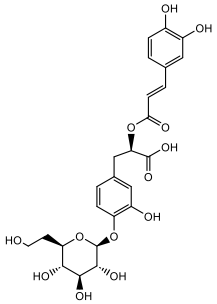
Molecular docking between 60 active-ingredient small-molecules of Sarcandra glabra and VEGFR-2 was accomplished. Twenty high-affinity ligands with TotalScore＞6 were acquired: four terpenoids, ten flavonoids, one coumarin and five phenolic-acid derivatives. Flavonoid molecules accounted for 47.62 % among high-activity candidates and exhibited superior overall binding affinity compared with other compound classes. Rosmarinic acid belonging to phenolic acids achieved the highest docking score (8.1064), representing the strongest binding stability toward VEGFR-2. These candidates proceeded to subsequent drug-likeness assessment (Table 2).

Table 2 Scoring table of high-affinity small-molecule ligands after virtual screening

No.	Name	Structure	Total sore
9	Chloranoside A		6.0544
17	Sarcaglaboside C		6.9605
18	Sarcaglaboside E		6.5002

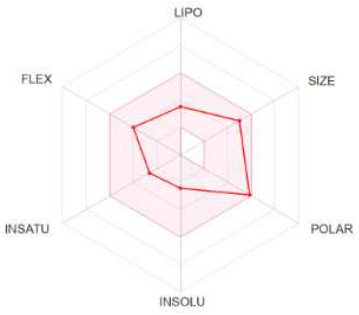
No.	Name	Structure	Total sore
19	Sarcaglaboside F		6.7892
22	GlabraosideA		6.1029
24	Catechin 3-O-α-L-rhamnopyranoside		6.0680
25	2',4' -dihydroxy-6'-methoxydihydrochalcone		6.0530
26	2',4'-dihydroxy-4,6'-dimethoxydihyrochalcone		6.3938
31	2',4',4-Trihydroxychalcone		6.0667
33	4',5-dibydroxy-7-methoxyflavanone		6.2608
34	（+）-3,3',5,5',7-pentahydroxyflavanone		6.8595
35	3,3',4',5,7-pentahydroxyflavone		6.6014

No.	Name	Structure	Total sore
36	Kaempferol-3-0-β-D-glucuronide		6.5586
38	Quercetin-3-O-β-D-glucuronopyranoside methyl ester		6.7553
50	Isofraxidin-7-O-β-D-glucopyranoside		6.1899
52	Rosmarinic acid		8.1064
53	Methyl rosmarinate		7.8275
55	Dibutyl phthalate		6.0291
56	Ethyl rosmarinate		7.4367

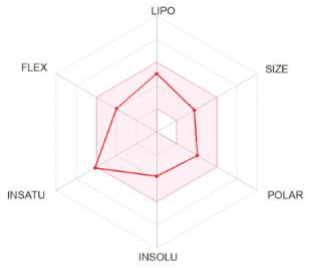
No.	Name	Structure	Total sore
57	4'-0-β-D-glucopyranosyl rosmarinic acid		6.9496

4.3 Drug-likeness screening results of active ingredients

The SwissADME bioavailability hexagon radar chart was adopted to intuitively visualize drug-likeness evaluation for 20 high-affinity ligands. The optimal druggable scope was defined by six descriptors: lipophilicity ($-0.7 < \text{LIPO} < 6.0$), molecular size ($150 < \text{SIZE} < 250$), polarity ($20\ \text{Å} < \text{POLAR} < 130\ \text{Å}$), solubility ($\text{INSOLU} < 6$), flexibility ($\text{FLEX} < 9$) and saturation ($\text{INSATU} > 0.25$) [8]. Five compounds fully satisfied all above criteria with balanced and favorable overall ADME-T profiles. Compound A (Sarcaglaboside C), Compound B (2',4'-dihydroxy-4,6'-dimethoxydihydrochalcone), Compound C (2'-hydroxy-4,4',6'-trimethoxy dihydrochalcone), Compound D ((+)-3,3',5,5',7-pentahydroxyflavanone), Compound E (isofraxidin-7-O-β-D-glucopyranoside) (Figure 1).



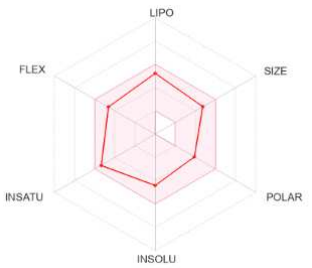
A



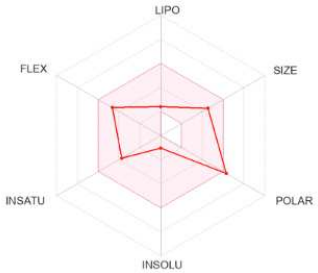
B



C



D



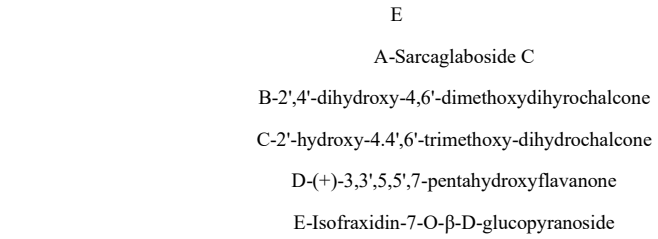


Figure 1 Radar chart of bioavailability for preferred ligands

4.4 Pharmacokinetic prediction results

ADMET druggability prediction and analysis were performed for the five candidate compounds (A-E) [9]. According to LogS grading criteria: $-6.00 < \text{LogS} < -4.00$ corresponds to soluble; $-4.00 < \text{LogS} < -2.00$ corresponds to highly-soluble. Except Compound E, all other candidates displayed favorable water-solubility, and Compound A exhibited optimal water-solubility performance.

In-silico prediction demonstrated that none of the five compounds acted as P-gp substrates, which reduced P-gp-mediated cellular efflux and favored intracellular drug accumulation. Blood-brain-barrier penetration was quantified via LogBBB grade: grade 0 = extremely high, grade 1 = high, grade 2 = moderate, grade 3 = low, grade 4 = undetermined. Compound A and E presented superior blood-brain-barrier permeability. LogPS (logarithm of blood-brain-barrier penetration surface area) reflects central-nervous-system penetration capacity; $\text{LogPS} < -3$ generally indicates poor central-nervous-system penetration. All five compounds met $\text{LogPS} < -3$, suggesting low risk of central-nervous-system exposure.

Cytochrome P450 (CYP450) represents key phase-I drug-metabolizing enzymes; inhibition on CYP450 subtypes may trigger drug-drug interactions and serves as a critical safety index for druggability [10]. Prediction results for major CYP450 subtypes revealed that Compound A and E did not inhibit CYP1A2, CYP2C9, CYP2C19, CYP2D6 or CYP3A4, whereas Compound B, C and D inhibited partial CYP450 isoforms. OCT2-substrate prediction indicated that none of five candidates were OCT2 substrates with low potential nephrotoxicity risk. Hepatotoxicity prediction showed zero predicted hepatotoxicity for all five candidates.

Collectively, Compound A (Sarcaglaboside C) achieved the optimal comprehensive performance in water-solubility, blood-brain-barrier permeability and metabolic stability, possessing superior drug-likeness properties (Table 3).

Table 3 Pharmacokinetic characteristics of screened compounds

NO.	Absorption			Distribution			Metabolism					Excretion	Toxicity
Compound	Log S (ESOL)	Log S (ALL)	Log S (SILICOS-IT)	P-glycoprotein inhibitor	Log BBB level	Log PS	CYP1A2	CYP2C9	CYP2D6	CYP2C19	CYP3A4	OCT2	Hepatotoxicity

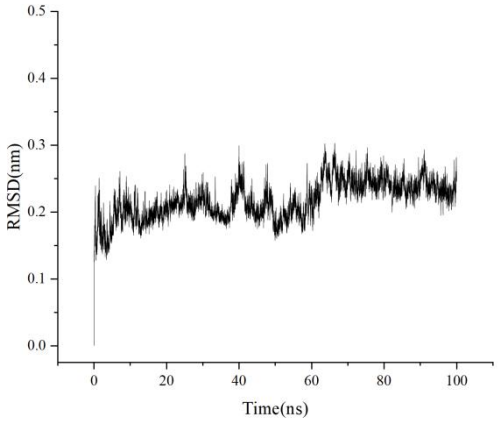
NO.	Compound	Absorption			Distribution			Metabolism						Excretion Toxicity	
		Log S (ESOL)	Log S (ALL)	Log S (SILICOS-IT)	P-glycoprotein inhibitor	Log BBB level	Log PS	CYP1A2	CYP2C9	CYP2D6	CYP2C19	CYP3A4		OCT2	Hepatotoxicity
A	Sarcaglaboside C	-2.07	-2.82	-2.56	-	2	-6.48	-	-	-	-	-		-	-
B	2',4'-dihydroxy-4,6'-dimethoxydihyrochalcone	-3.62	-3.79	-3.62	-	3	-6.72	+	+	+	-	+		-	-
C	2'-hydroxy-4.4',6'-trimethoxy-dihydrochalcone	-3.22	-4.00	-3.41	-	3	-5.84	+	+	+	+	+		-	-
D	(+)-3,3',5,5',7-pentahydroxyflavanone	-4.16	-4.41	-4.28	-	4	-6.20	-	+	+	-	-		-	-
E	Isofraxidin-7-O-β-D-glucopyranoside	-6.78	-6.03	-6.16	-	1	-7.12	-	-	-	-	-		-	-

+—Positive,-—Negative.

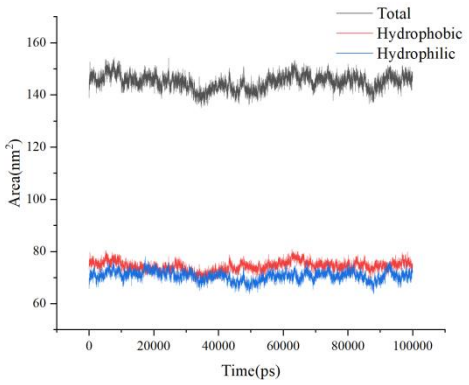
4.5 Molecular-dynamics-simulation results for protein-ligand complex

To predict binding affinity between Sarcaglaboside C and VEGFR-2 protein, the VEGFR-2-Sarcaglaboside-C complex model was constructed and subjected to MD simulation. Root-mean-square-deviation (RMSD) of protein backbone fluctuated markedly during the initial 0-60 ns, corresponding to conformational relaxation of the system. RMSD tended to stabilize and fluctuated within 0.20-0.28 nm after 60 ns, implying that the system reached dynamic equilibrium in later simulation stages. Small-molecule ligands adjusted conformation and formed stable dominant binding geometry. Amino-acid residues interacting with Sarcaglaboside C maintained overall conformational stability, verifying that Sarcaglaboside C could stably occupy the substrate-binding pocket of VEGFR-2 protein. Solvent-accessible-surface-area (SASA) analysis

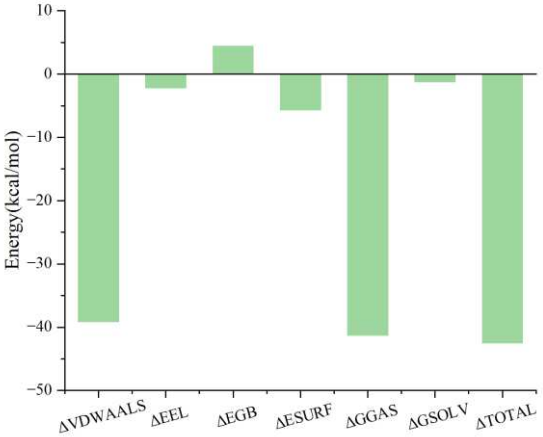
for protein-ligand complex: total SASA of complex remained stable at 140-152 nm² throughout the 100-ns simulation. Both hydrophobic and hydrophilic SASA fluctuated steadily within 70-80 nm without obvious unidirectional shifts. It demonstrated that ligands stayed anchored within protein pockets without obvious dissociation or large-scale conformational rearrangement; hydrophobic-hydrophilic surface partitioning of complexes remained stable. The molecular mechanics-generalized-Born-surface-area (MM-GBSA) approach was used for binding-free-energy calculation of protein-ligand complex. The total binding free energy of system reached −42.51 kcal/mol, indicating spontaneous formation of stable protein-ligand complex. Gas-phase free energy ΔG_{GAS} (−41.30 kcal/mol) constituted the major driving-force for binding, among which van-der-Waals interaction (ΔVDWAALS = −39.12 kcal/mol) dominated complex stabilization, while gas-phase electrostatic contribution (ΔEEL = −2.18 kcal/mol) was weak. Solvation free energy ΔG_{SOLV} was −1.20 kcal/mol. Non-polar solvation contribution (ΔESURF = −5.64 kcal/mol) favored binding, whereas polar solvation term (ΔEGB = 4.44 kcal/mol) disfavored binding and partially counterbalanced electrostatic interactions. In summary, van-der-Waals forces together with hydrophobic effects maintained stable complex assembly (Figure 2).



A—The diagram of RMSD



B—The diagram of SASA



C—The diagram of RMSD MM-GBSA

Figure 2 .Molecular dynamics simulation of Sarcaglaboside C with VEGFR-2

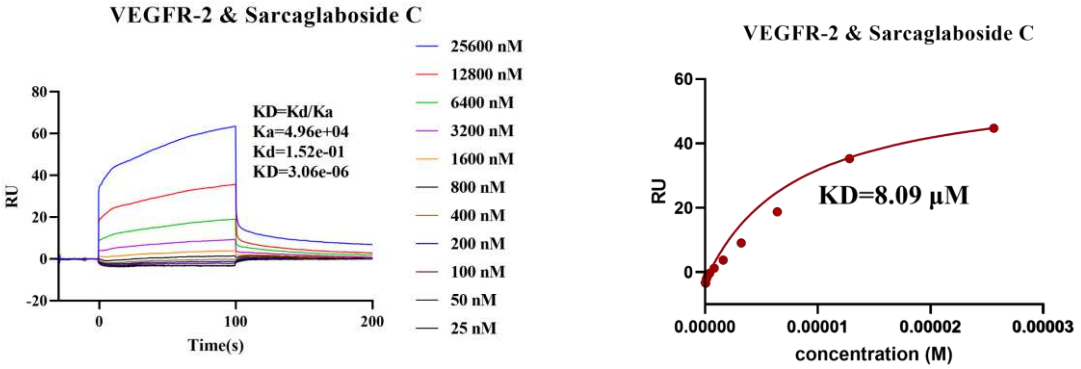
4.6 Detection results from surface-plasmon-resonance assay

SPR technology was applied to evaluate direct molecular interaction between Sarcaglaboside C and VEGFR-2 protein. Sensorgrams displayed obvious SPR responses upon injecting Sarcaglaboside C over VEGFR-2-immobilized chip surfaces within concentration range of 25-25 600 nM. Response signals increased in a concentration-dependent manner. Obvious binding process was observed in association phase for all concentrations; maximum response value of approximately 60 RU was achieved at highest concentration (25 600 nM).

Figure A of the kinetic fitting results shows that the association rate constant of sarcaglaboside C binding to VEGFR-2 is ka =4.96×10^4 $M^{-1} \cdot s^{-1}$, the dissociation rate constant is Kd=1.52 $M^{-1} \cdot s^{-1}$, and the corresponding kinetic equilibrium dissociation constant KD=3.06× 10-6M), equivalent to approximately 3.06 μM.

Figure B from steady-state affinity analysis demonstrates that the equilibrium binding response (RU) increases gradually with rising concentrations of sarcaglaboside C. At low concentrations, the response rises rapidly as concentration increases; upon further concentration elevation, the increment in response declines, and the fitted curve exhibits a typical concentration-dependent binding trend approaching saturation. The steady-state fitting yields a KD of 8.09 μM, which further indicates stable binding capacity between Sarcaglaboside C and VEGFR-2.

Steady-state affinity analysis demonstrated that equilibrium-binding response (RU) increased with compound concentration. Response values climbed rapidly under low-concentration conditions, and the increment gradually slowed at higher concentrations. Fitting curves exhibited typical concentration-dependent saturation-binding tendency. Steady-state fitted KD value was 8.09 μM, further confirming stable binding capacity of Sarcaglaboside C toward VEGFR-2 protein.



A—The sensor diagram of Sarcaglabosid C with VEGFR-2 B—The Fitted curve of Sarcaglabosid C with VEGFR-2

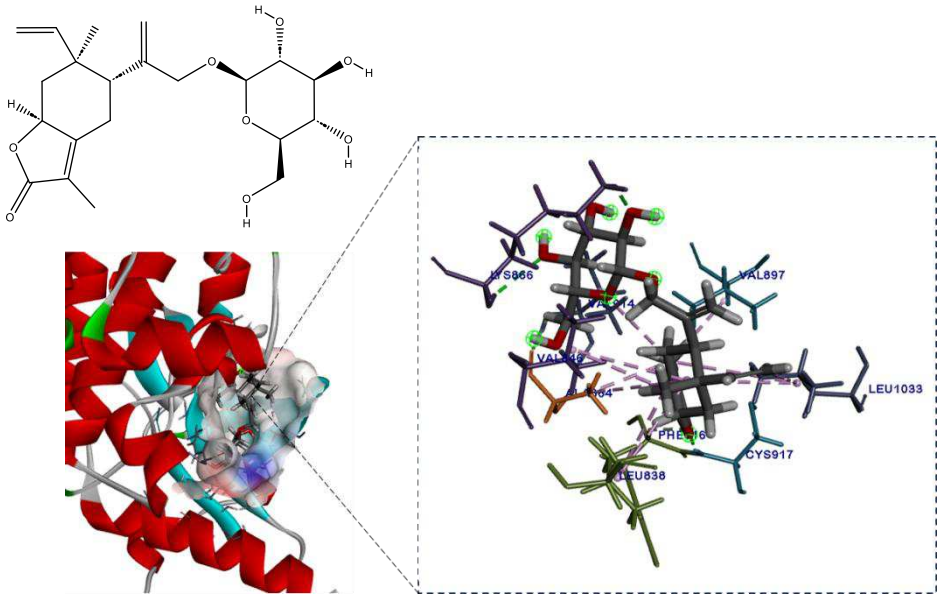
Figure 3. Sarcaglabosid C with VEGFR-2 binding kinetics curve

4.7 Molecular-docking interaction analysis

Molecular docking was used to further interpret interaction patterns between Sarcaglaboside C and VEGFR-2 protein. Sarcaglaboside C could insert deeply inside the protein-binding cavity (Figure A). The carbonyl oxygen on the lactone ring of Sarcaglaboside C formed hydrogen-bond contacts with Cys917; hydroxyl groups on sugar moiety established hydrogen-bond interactions with Lys866 amino-acid residues (Figure B). Sarcaglaboside C fitted completely within the VEGFR-2 binding pocket. Its hydrophobic parent nucleus and polar glycosyl groups matched well with hydrophobic and hydrophilic micro-regions of pocket respectively without significant steric hindrance. Hydrogen-bond and hydrophobic effects synergistically stabilized protein-small-molecule complex system (Figure C).

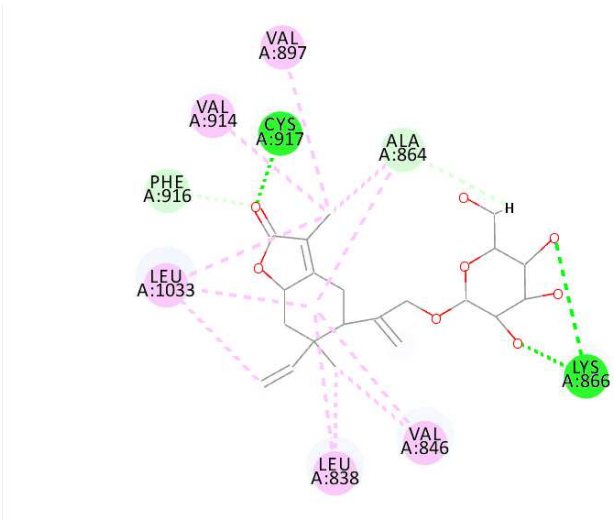
Compared with original ligand of VEGFR-2, Cys917 and Lys866 acted as characteristic hydrogen-bond-forming residues for Sarcaglaboside C, while hydrophobic amino-acid residues including Val and Leu maintained stable anchoring of small-molecule within active pocket. SwissADME druggability prediction revealed favorable drug-likeness for Sarcaglaboside C. Its terpenoid parent-skeleton plus glycosyl moiety can serve as lead-compound scaffold for subsequent structural modification. Alterations on side-chain substituents are expected to adjust lipophilic-hydrophilic partition coefficient, improve in-vivo bioavailability and further elevate anti-tumor activity.

A

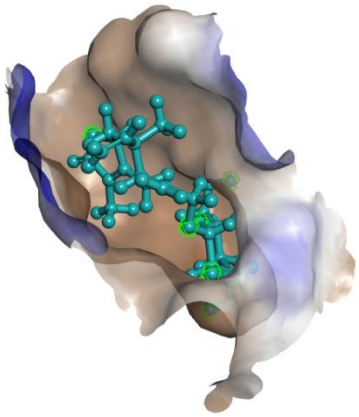


A—3D of Sarcaglaboside C binding to VEGFR-2 amino acid residues

B



B—2D of Sarcaglaboside C binding to VEGFR-2 amino acid residues



C—3D Hydrophobicity of Sarcaglaboside C binding to VEGFR-2 amino acid residue

Figure 4. The Sarcaglaboside C and VEGFR-2

5. Discussion

In this study, 60 small-molecule ligands derived from Sarcandra glabra were subjected to molecular docking evaluation against the VEGFR-2 target protein, as well as predictions of drug-likeness, oral bioavailability and pharmacokinetic properties. The screening results revealed that Sarcaglaboside C exhibited the optimal drug-like properties and possessed the strongest binding capacity to VEGFR-2 among all candidate compounds. Subsequent molecular dynamics simulations further confirmed stable intermolecular interactions between this compound and VEGFR-2, which verified the reliability of the computer-aided virtual screening and model evaluation adopted in the present work. Existing pharmacological studies on Sarcandra glabra have indicated that sesquiterpene glycosides from the genus Sarcandra possess potential values for inhibiting tumor cell proliferation and inducing cell apoptosis. As a member of the sarcaglaboside-type sesquiterpene glycosides, Sarcaglaboside C belongs to this compound family. It has been reported that sesquiterpene constituents from the same genus can regulate apoptosis-related signaling pathways including PI3K/Akt and Bax/Bcl-2 [11-13], and exert in-vitro inhibitory effects on tumor cells such as hepatocellular carcinoma and leukemia cells.

In addition, the 60 compounds shared partial structural similarity with ketone-carbonyl and hydroxyl active groups. Docking TotalScore values positively correlated with hydroxyl-group counts in molecules, which may be attributed to that hydroxyl groups readily form hydrogen-bonds with amino-acid residues of target protein. According to drug-likeness and lead-like prediction, Sarcaglaboside C can be developed as lead compound. However, relatively weak biomembrane-affinity restricts its bioavailability. Based on molecular-docking results, the terpenoid parent-skeleton and glycosyl-group structural features can be taken as core scaffolds for structural derivatization to enhance molecular lipophilicity and improve anti-tumor pharmacological potency.

The present work merely accomplished protein-level binding validation. SPR experiments only demonstrated physical binding between small-molecule and VEGFR-2 protein. Kinase-inhibition assays, cellular and in-vivo anti-tumor pharmacological experiments have not yet been performed. Hence, we cannot confirm kinase-inhibitory function or cellular anti-tumor activity of Sarcaglaboside C. Further kinase-activity determination, cellular angiogenesis

phenotype assays are required to validate functional activity. Structural modification will be implemented based on this scaffold to optimize druggability properties.

6.Conclusion

In this study, molecular docking was performed between the VEGFR-2 target protein and 60 bioactive small molecules derived from Sarcandra glabra. Analysis of the TotalScore values revealed that flavonoids exhibited superior overall binding affinity among the high-affinity candidates, presumably owing to the ketone carbonyl and hydroxyl functional groups commonly present in these molecules, which readily form stable hydrogen bonds with amino acid residues of the target protein.

The screened high-affinity compounds were subsequently subjected to drug-likeness, bioavailability, and ADMET predictions. The results demonstrated that Sarcaglaboside C possessed the most favorable drug-like properties, and molecular docking analysis revealed that it forms hydrogen-bond interactions with the key amino acid residues Cys917 and Lys866. The binding affinity between Sarcaglaboside C and VEGFR-2 was further verified by in vitro surface plasmon resonance (SPR) assays using a Biacore system, yielding a kinetic equilibrium dissociation constant (K_D) of 3.06 μM and a steady-state fitted K_D of 8.09 μM. These experimental findings validated the accuracy of the computer-aided virtual screening and model evaluation, thereby enhancing the efficiency of drug discovery.

Furthermore, the identified Sarcaglaboside C can serve as a lead compound for structural optimization. Given that its relatively weak biomembrane affinity limits in vivo bioavailability, structural modifications can be undertaken by exploiting the multiple reactive groups present in its molecular scaffold. By targeting VEGFR-2, this study identified the optimal active constituent from Sarcandra glabra, providing a theoretical basis for elucidating the anti-tumor mechanisms of Sarcandra glabra bioactive ingredients. The findings also offer a promising lead compound for the subsequent development of small-molecule inhibitors targeting vascular endothelial growth factor receptor-2.

Declarations

Ethics declaration not applicable.

Competing interests The authors declare that they have no known competing financial interests or personal relationships that could have appeared to influence the work reported in this paper.

Funding Not applicable.

Authors' contributions Wen Xing: Conceptualization, Methodology, Software, Formal analysis, Writing – original draft. Guo-zhu Gao: Data curation, Investigation, Validation. Fan-yuan Jia: Investigation, Resources. Zhen-Yu Kuai: Methodology, Validation, Writing – review & editing. Yan-Qiu Meng: Supervision, Project administration, Writing – review & editing. All authors have read and agreed to the published version of the manuscript.

Acknowledgements Not applicable.

References

[1] Zhou BX, Hua H, Liu M. Research progress on clinical anti-tumor efficacy and action mechanism of *Sarcandra glabra*[J]. Shanghai Journal of Traditional Chinese Medicine, 2023, 57(11):85-89.

[2] Wei CM, Zhang JJ, Li BY. Research progress on natural compounds targeting VEGF/VEGFR for anti-tumor therapy[J]. Chinese Herbal Medicines, 2017, 48(23):5049-5056.

[3] Zhu P, Hu C, Hui K, et al. The role and significance of VEGFR-2 regulatory T cells in tumor immunity [J]. Onco Targets Ther, 2017,10:4315-4319.

[4] Kuai ZY, Wu LY, Zeng X, et al. Anti-tumor screening and activity study of flavonoids from Astragalus based on PTK target[J]. Journal of Shenyang Pharmaceutical University, 2025,42 (2):162-169.

[5] Harris P A, Cheung M, Hunter R N, et al. Discovery and Evaluation of 2-Anilino-5-aryloxazoles as a Novel Class of VEGFR-2 Kinase Inhibitors[J]. Journal of Medicinal Chemistry, 2005, 48(6): 1610–1619.

[6] Tang B, Wang H X, Fu X L, et al. Virtual screening of TGF-B1 inhibitors of Chinese materia medica small molecule based on discovery studio platform[J]. Chin J Tradit Chin Med Pharm,2021,36(11):6669-6673.

[7] Madison W E, Tara W H, Brian A S,et al. Use of in-silico assays to characterize the ADMET profile and identify potential therapeutic targets of fusarochromanone, a novel anti-cancer agent[J]. In Sil Pharm,2015,3(1):6.

[8] Hu B C, Tian J X, Zhang Y T, et al. Online prediction of compound's drug ability [J]. Chinese Journal of Medicinal Chemistry,2022,32(2):90-101.

[9] Ritchie T J, Ertl P, Lewis R. The Graphical Representation of ADME-Related Molecule Properties for Medicinal Chemists [J]. Drug Discovery Today,2011,16(1/2):65-72.

[10] Manikandan P, Nagini S. Inhibition and induction of CYP enzymes in humans: an update[J]. Archives of Toxicology, 2018, 92(11):3295-3322.

[11] Weddell J C, Chen S, Imoukhuede P I. VEGFR-1 promotes cell migration and proliferation through PLCγ and PI3K pathways[J]. Syst Biol Appl,2018,4:1-11.

[12] Zhou BX, Hua H, Liu M. Research progress on clinical anti-tumor efficacy and action mechanism of *Sarcandra glabra*[J]. Shanghai Journal of Traditional Chinese Medicine, 2023,57(11):85-89.

[13] Zhou B, Liu KY, Chang J, et al. Advances in chemical constituents and pharmacological effects of *Sarcandra glabra*[J]. Chinese Journal of Modern Applied Pharmacy,2009,26(12):982-986.